VISSR ATMOSPHERIC SOUNDER

Monthly Progress Report No. 9
For the Period 1 May 1974 to 31 May 1974

Contract No. NAS5-21965

For National Aeronautics and Space Administration
Goddard Space Flight Center
Glen Dale Road
Greenbelt, Maryland 20771

By

V. E. Suomi, Principal Investigator
L. A. Sromovsky, Co-Investigator

The University of Wisconsin
Space Science and Engineering Center
1225 West Dayton Street
Madison, Wisconsin 53706

Introduction

During the past month, the VAS simulator has been producing useful results. However, the results have not yet been summarized and analyzed. The first installment will appear in the June or July report. As a preface to that, we are including here a description of the radiance grids ("scenes") used in the simulator.

A second area of effort has been the VAS in-flight calibration. During the past month, the possibility of using an internal space-view to improve the VAS calibration has been partially analyzed. The results discussed in the second section of this report indicate that dependence on telescope temperature measurements cannot be eliminated.

1. VAS Simulator Scene Description

The scene used for the simulation of VAS measurements which will be reported on in future reports is the Canary Islands cloud grid derived from Gemini photographs which has been discussed previously. The altitudes and emissivities of the two cloud types contained in the grid are given in Table 1. along with the cloud radiances for each channel.

The total Canary Islands grid contains an area about 360 km square. Subgrids of this area which are 90 x 90 km have been used extensively for simulation. Thus, it is useful to break down the scene characteristics by subgrid (labelled from 1-16 and located consecutively from left to right as words on the printed page). Contour plots of the window channel radiances of the subgrids are shown in Figures 1. a-p. It is evident that a great variety of cloud shapes, sizes and coverage are represented in the subgrids, as well as a substantial amount of cloud mising. The cloud cover characteristics of each subgrid are listed in Table 2. It should be noticed that the

TABLE 1. Canary Island Cloud Types

Cloud A: altitude = 800 mb; = .80

Cloud B: altitude = 350 mb; = .85

(Transmission Coefficient) = 0)

		Radiances (ergs/etc)	
CHANNEL	CLEAR	CLOUD A	CLOUD B
1	10.737	10.737	10.651
2	14.345	14.181	11.737
3	27.844	25.814	16.162
4	37.478	32.233	18.134
5	79.222	54.497	23.859
6	99.754	62.072	25.106
7	101.608	61.309	23.800
8	89.895	53.211	18.780
9	31.495	17.136	3.991
10	23.172	12.336	2.662
11	1.395	.618	.066
12	.383	.156	.013

TABLE 2. Subgrid Cloud Cover

Cloud Percents in the Scene Grid

SUBGRID	% CLOUD A	% CLOUD B	% CLEAR	% CLEAR SOUNDER SAMPLES*
1	9	13	79	3
2	2	1	97	45
3	15	7	78	4
4	14	15	71	3
5	16	7	77	2
6	10	19	71	1
7	20	13	67	0
8	5	23	72	7
9	21	9	70	8
10	6	13	73	2
11	13	6	81	0
12	4	1	95	17
13	19	40	41	0
14	11	12	77	3
15	22	21	57	1
16	17	28	55	0
AVERAGE	13	14	73	6

* A clear sounder sample was defined to be a totally clear area of 8 mr in the east-west direction and 4mr north-south. (30 km x 15 km). There are 150 samples/subgrid in the simulator.

Figure 1.a- CHANNEL 8 SCENE RADIANCES (SUBGRID 1)

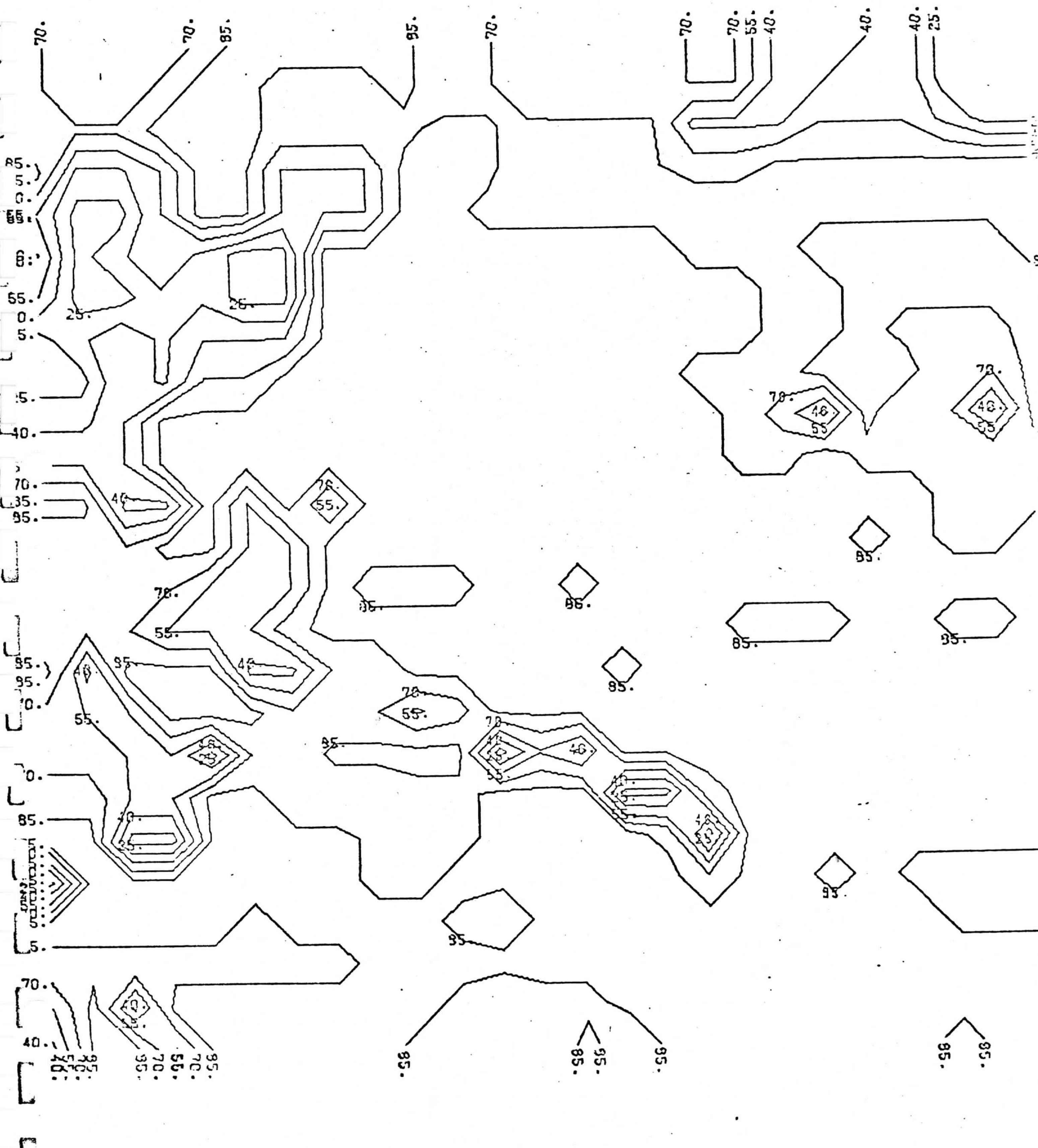

Figure 1.b CHANNEL 8 SCENE RADIANCES (SUBGRID 2)

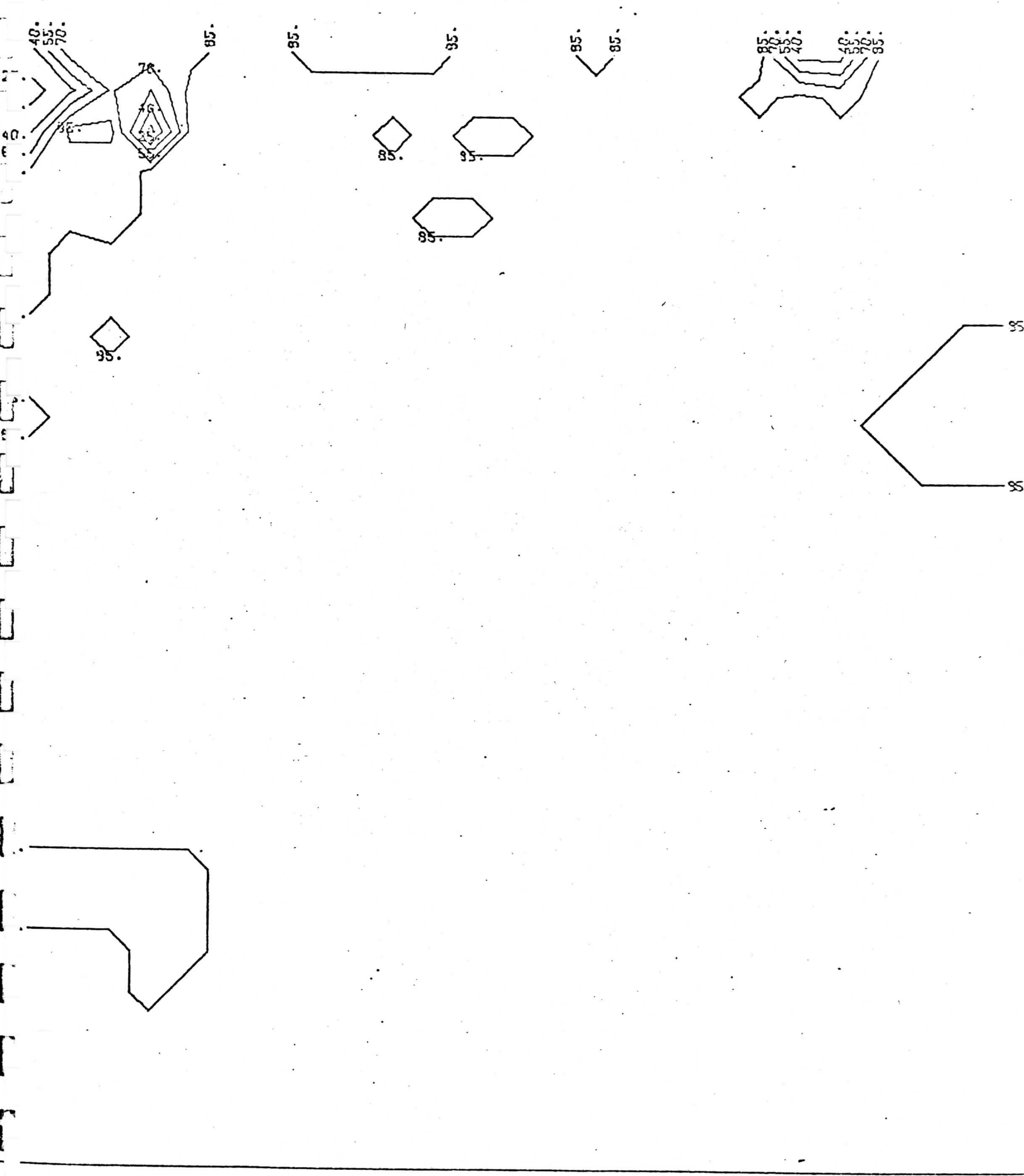

Figure 1.c CHANNEL 8 SCENE RADIANCES (SUBGRID 3)

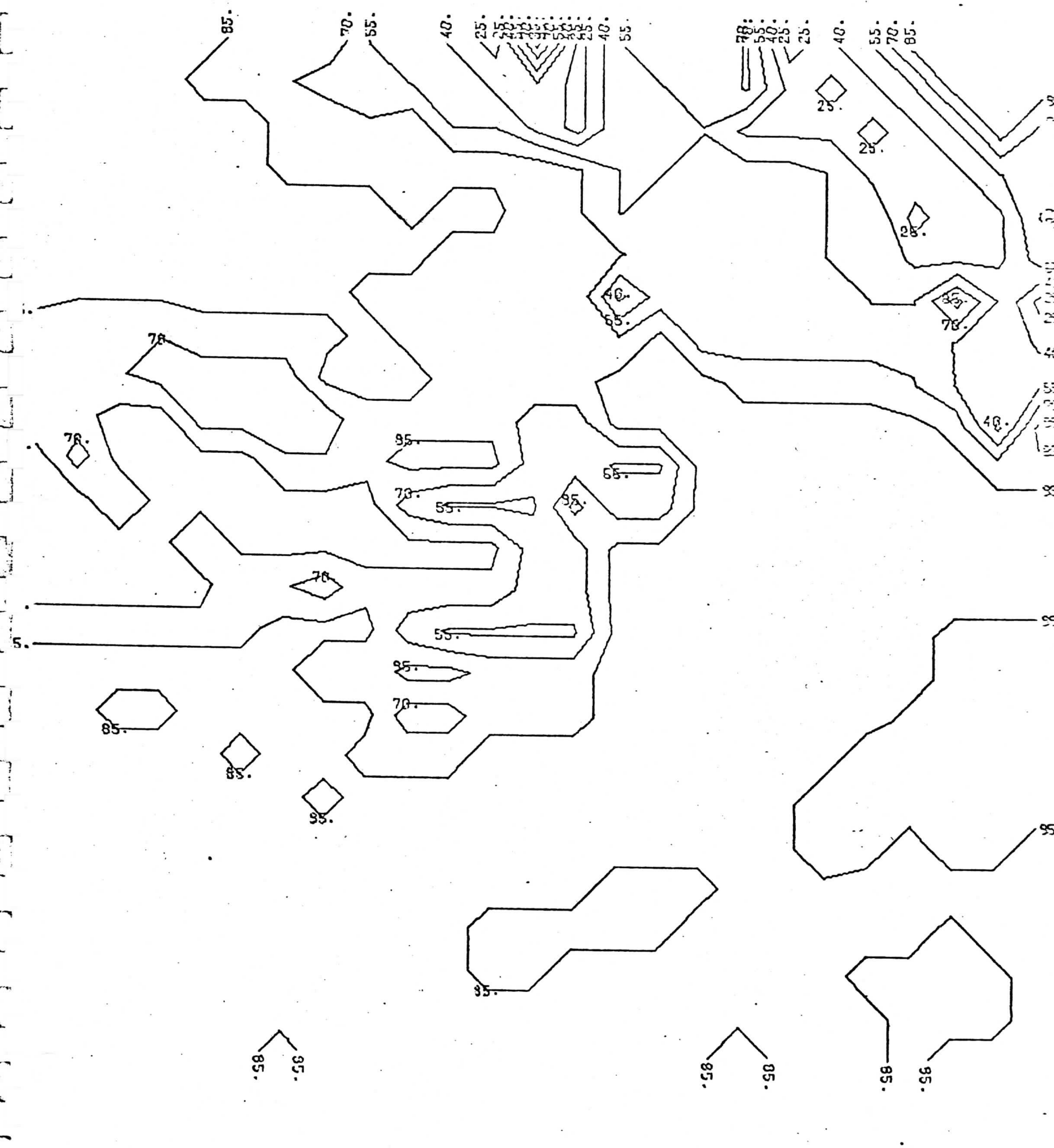

Figure 1.d CHANNEL 8 SCENE RADIANCES (SUBGRID 4)

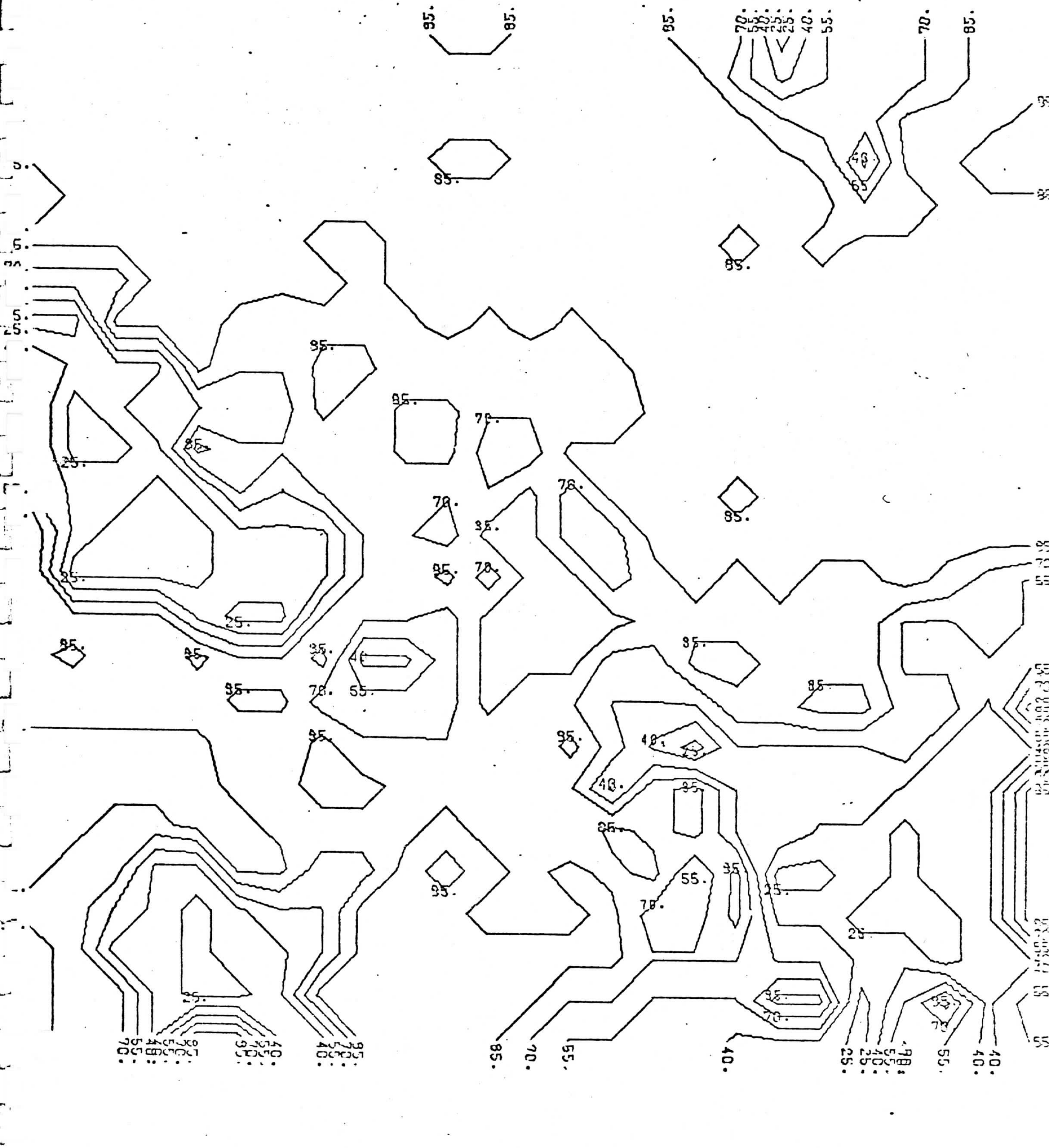

Figure 1.e CHANNEL 8 SCENE RADIANCES (SUBGRID 5)

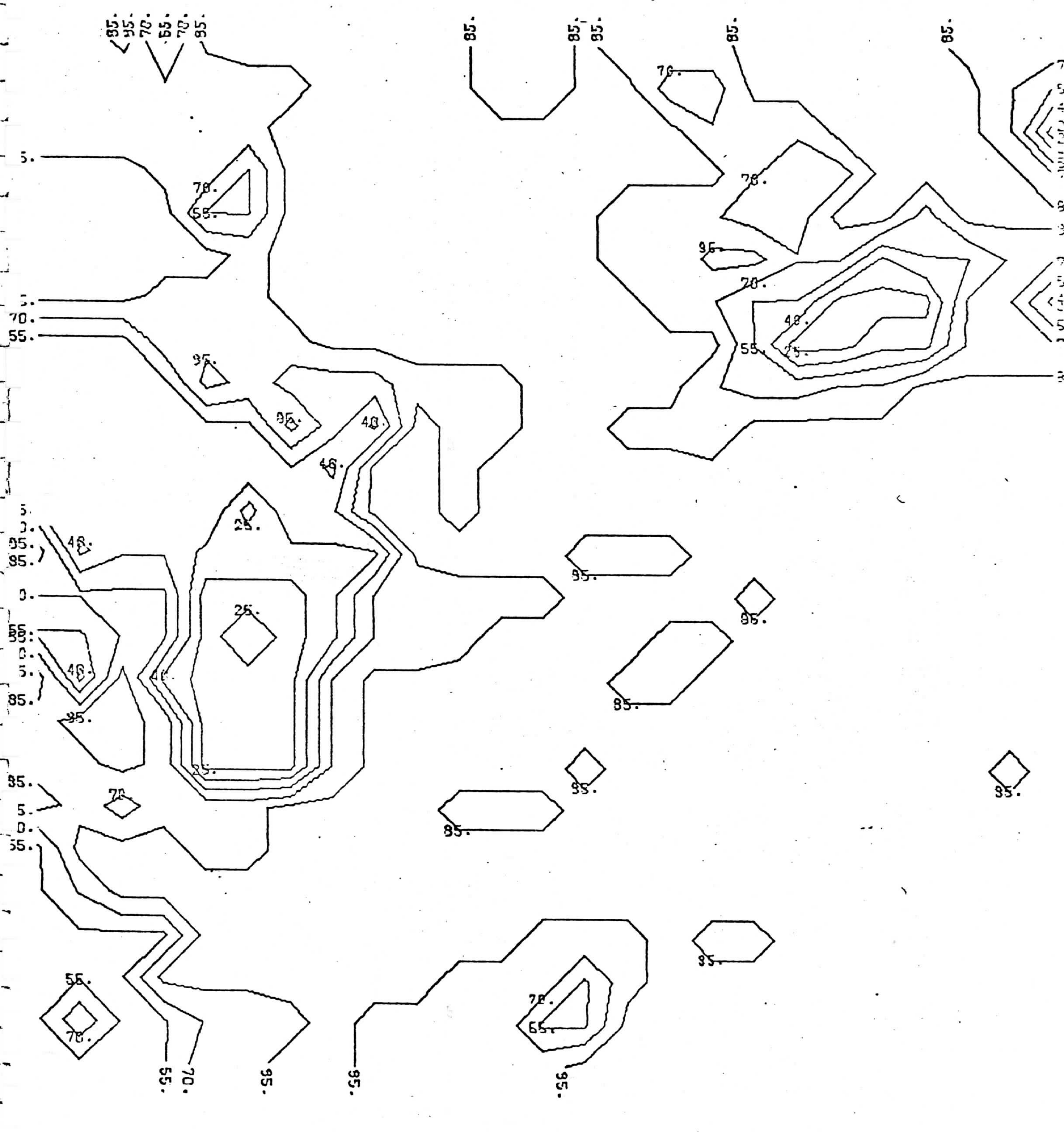

Figure 1.f CHANNEL 8 SCENE RADIANCES (SUBGRID 6)

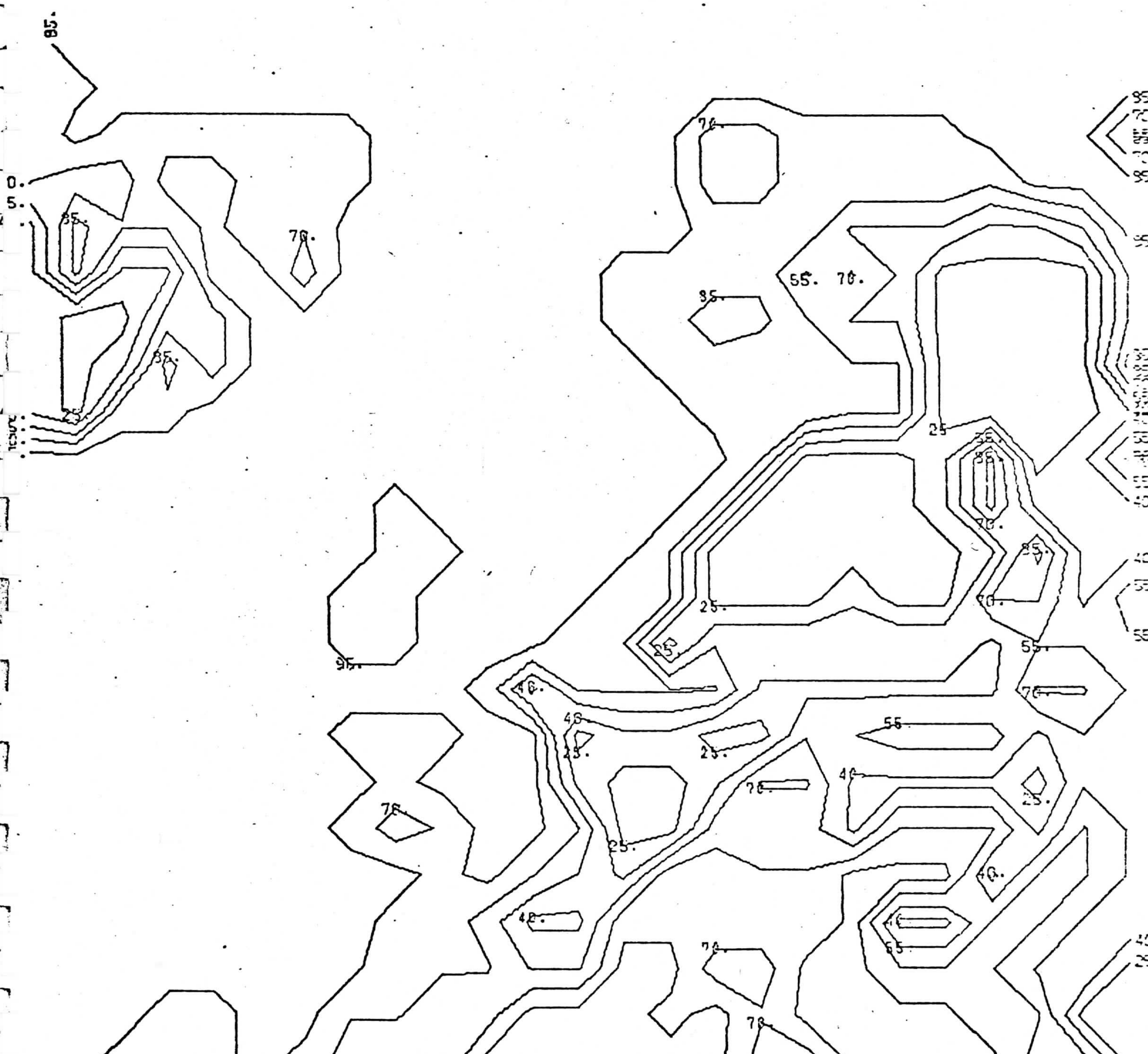

Figure 1.g CHANNEL 8 SCENE RADIANCES (SUBGRID 7)

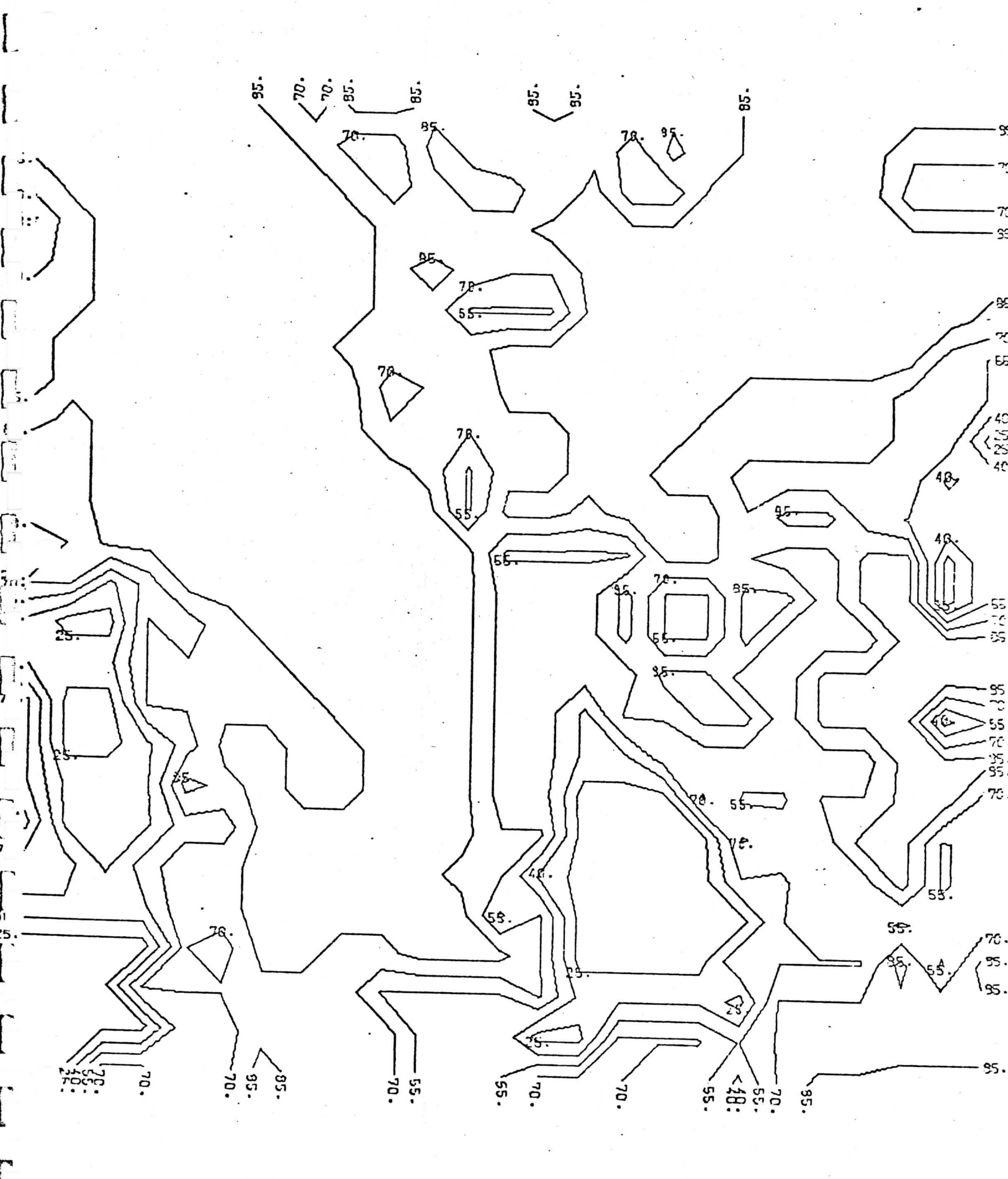

Figure 1.h CHANNEL 8 SCENE RADIANCES (SUBGRID 8)

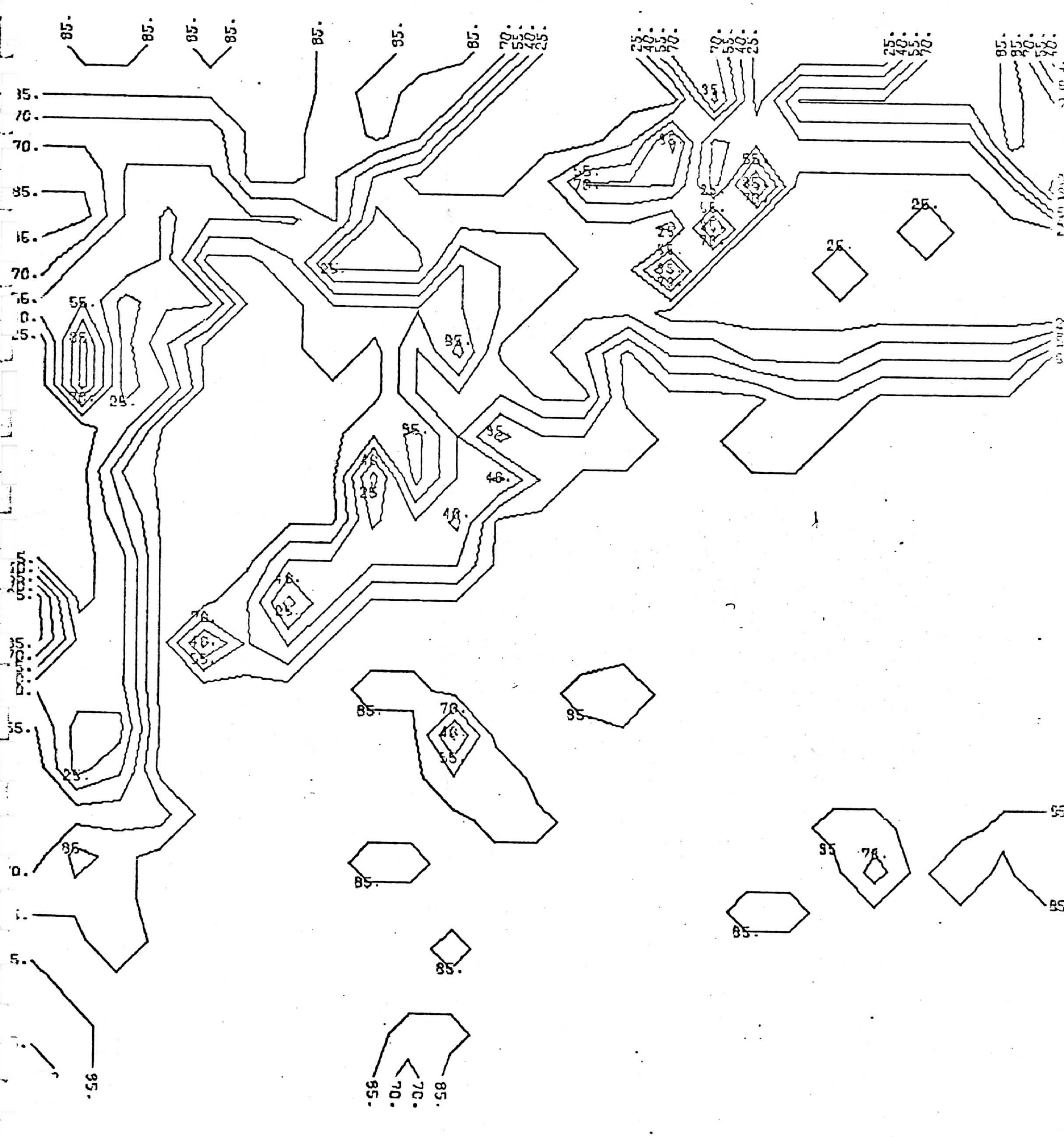

Figure 1.1 CHANNEL 8 SCENE RADIANCES (SUBGRID 9)

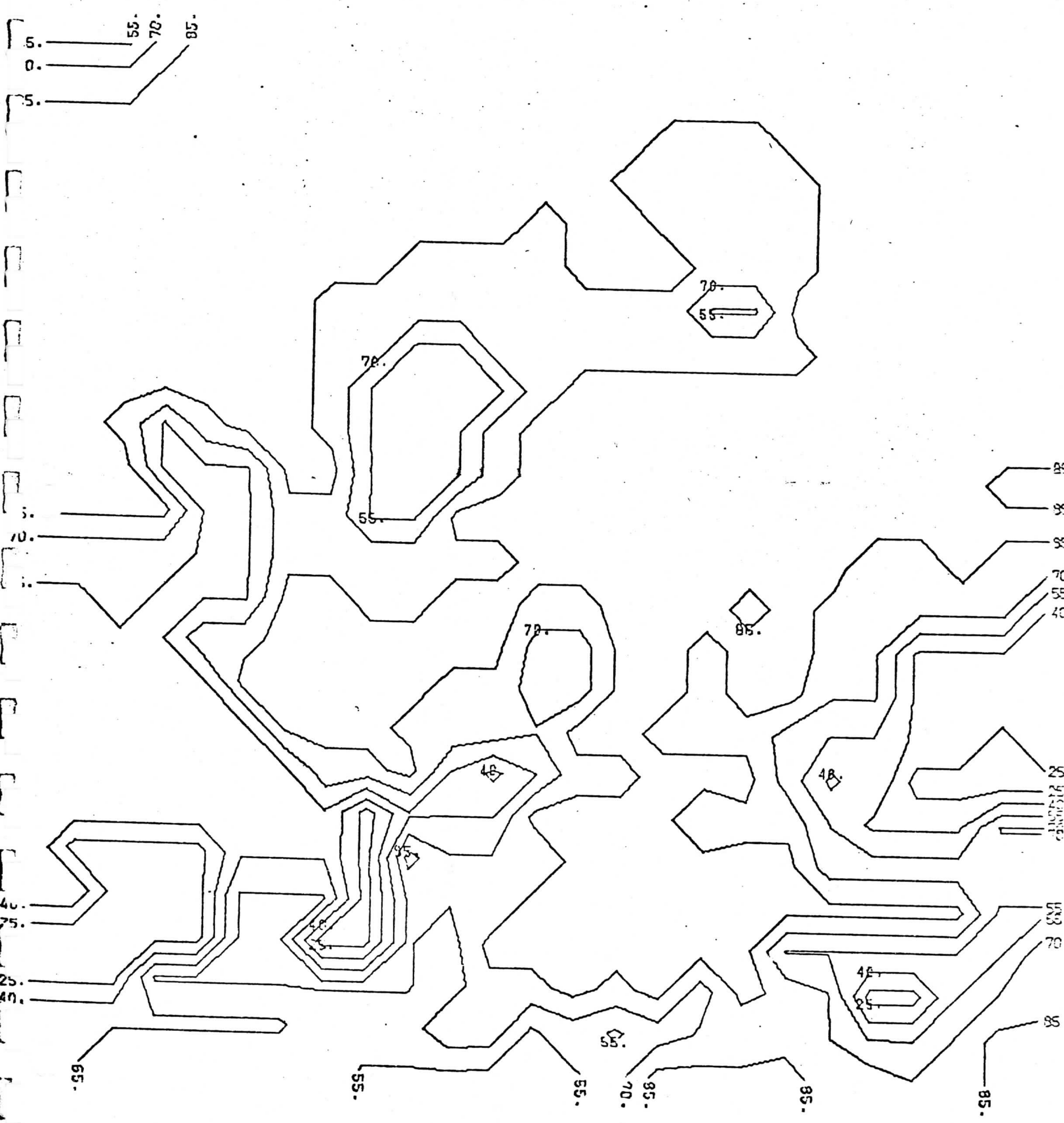

Figure 1.j CHANNEL 8 SCENE RADIANCES (SUBGRID 10)

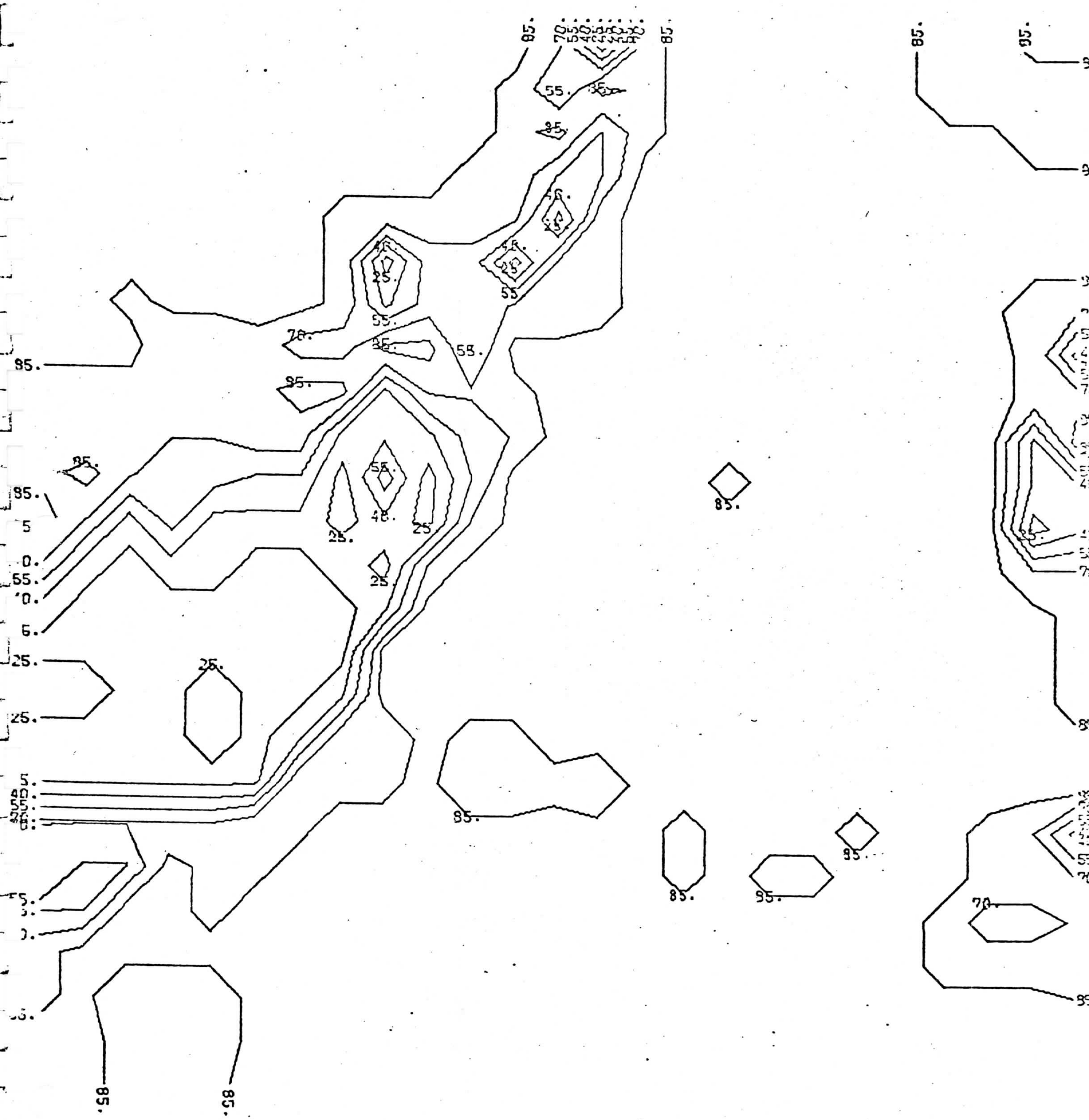

Figure 1.k CHANNEL 8 SCENE RADIANCES (SUBGRID 11)

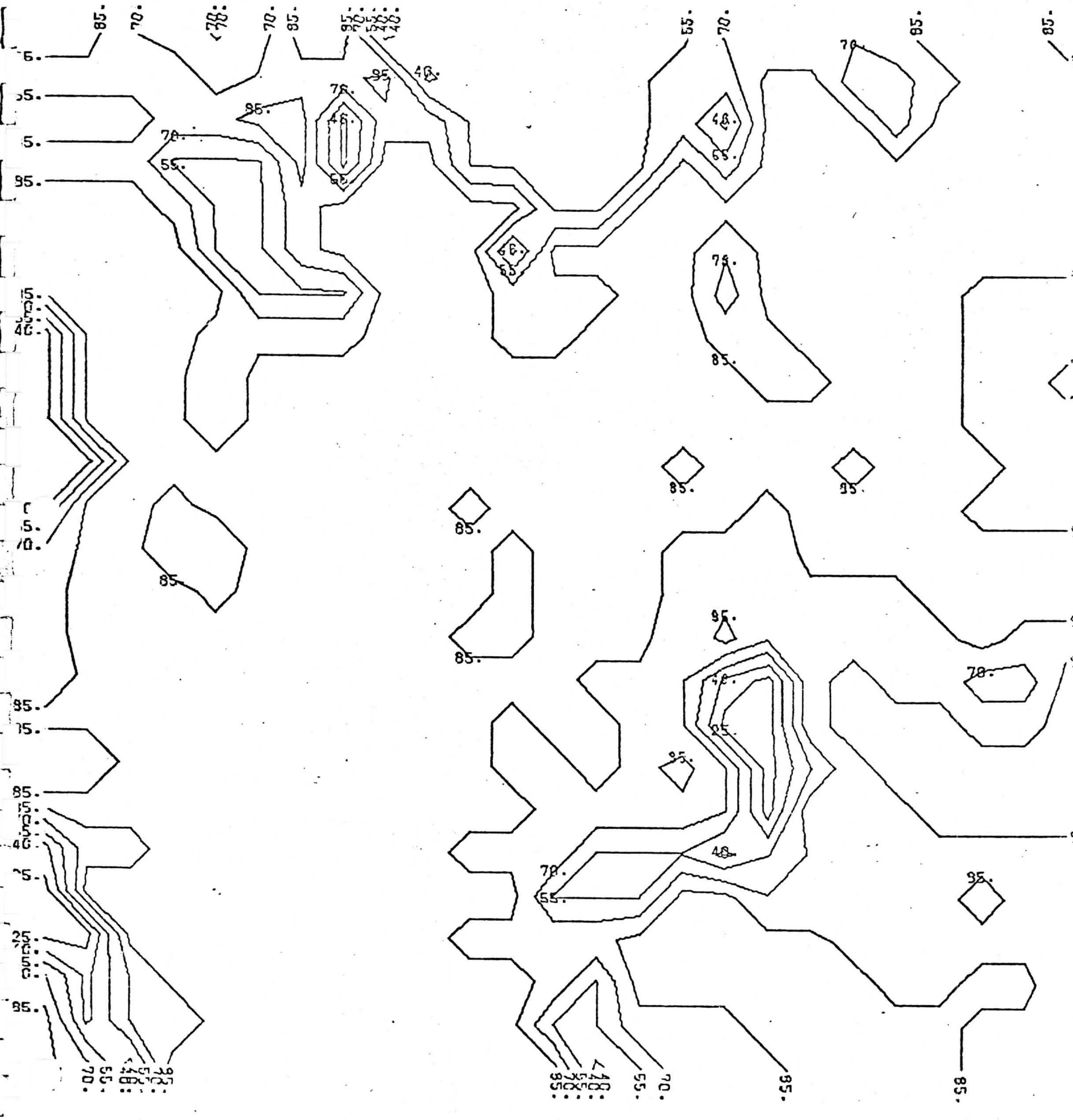

Figure 1.1 CHANNEL 8 SCENE RADIANCES (SUBGRID 12)

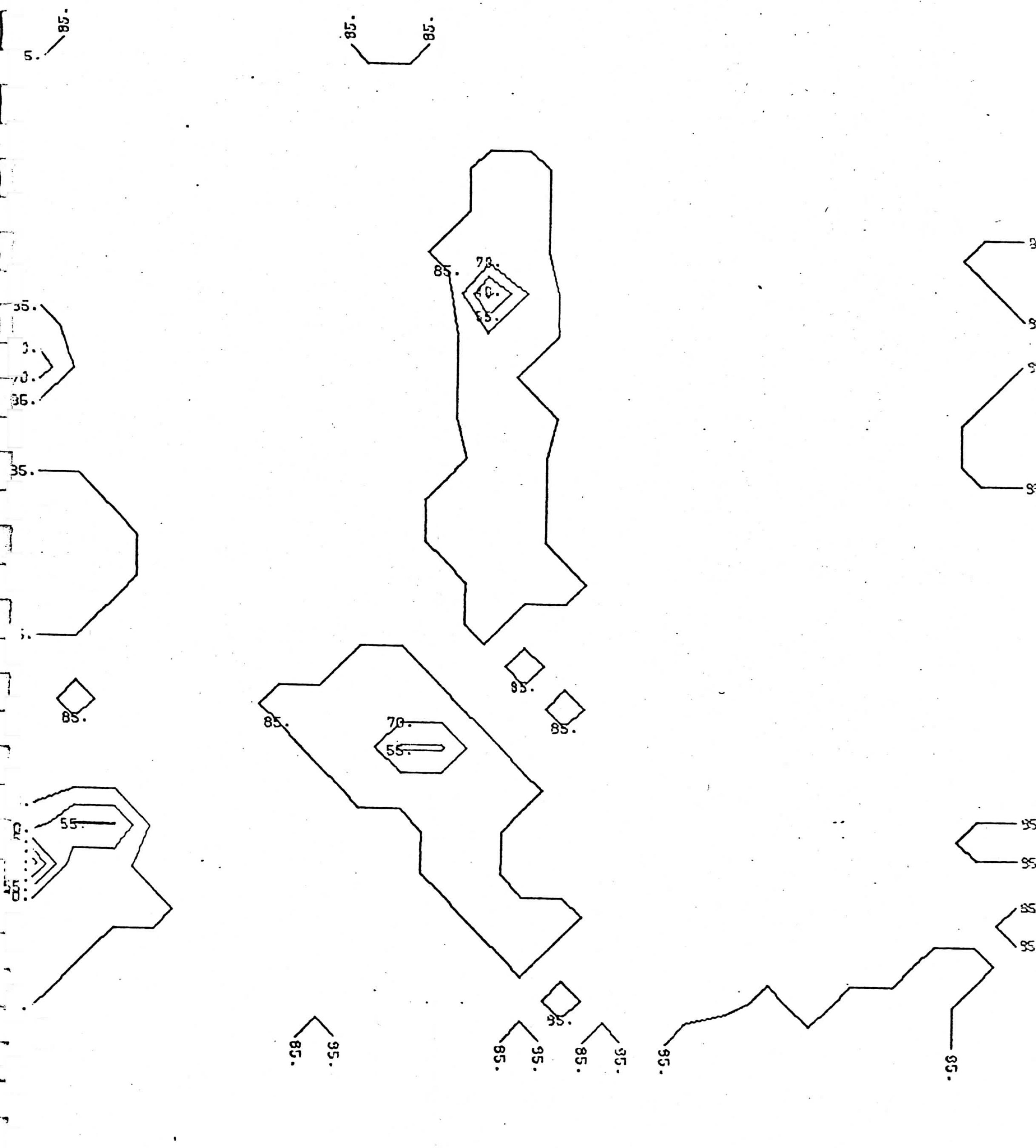

Figure 1.m. CHANNEL 8 SCENE RADIANCES (SUBGRID 13)

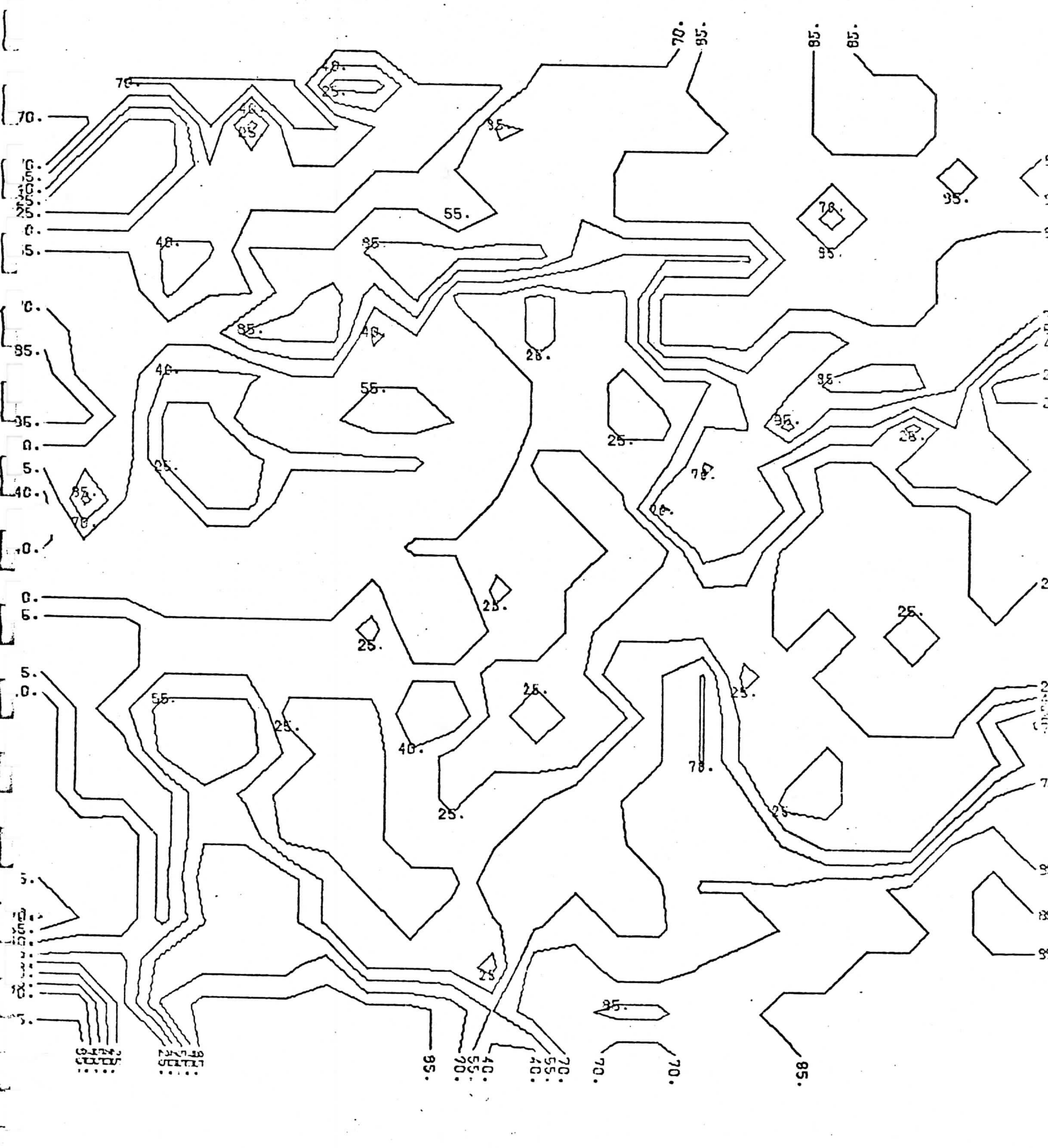

Figure 1.n CHANNEL 8 SCENE RADIANCES (SUBGRID 14)

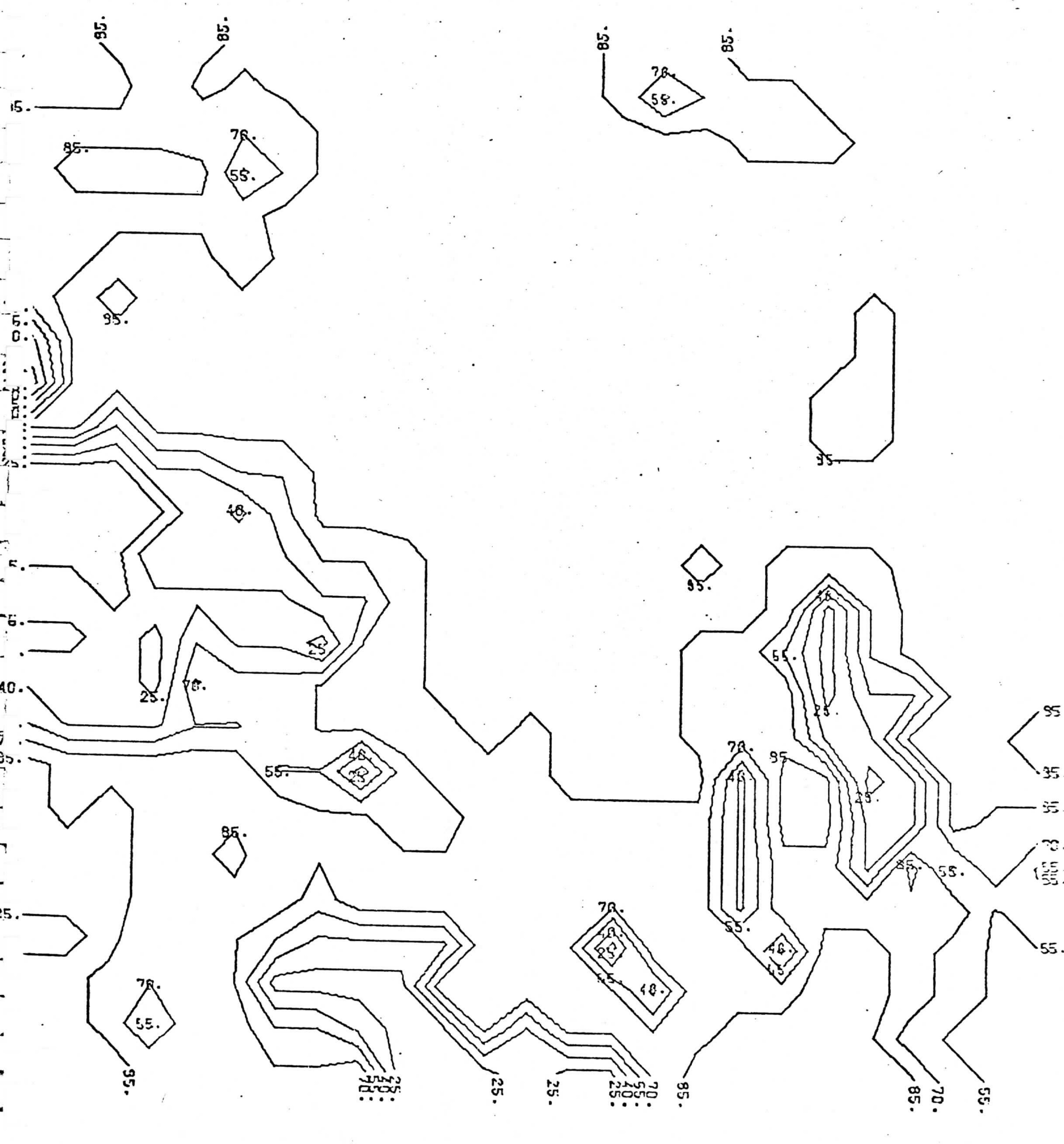

Figure 1.o CHANNEL 8 SCENE RADIANCES (SUBGRID 15)

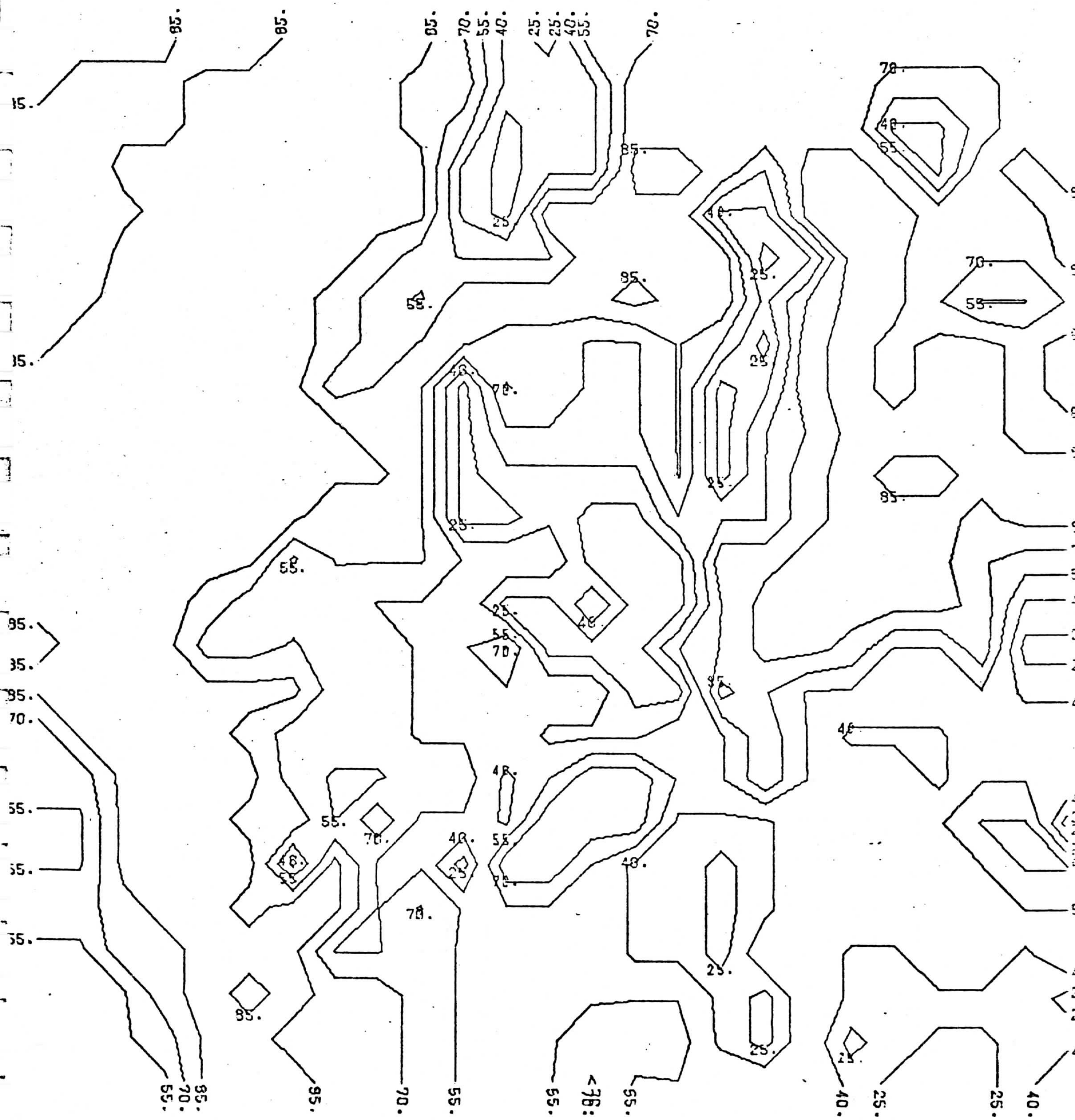

Figure 1.p CHANNEL 8 SCENE RADIANCES (SUBGRID 16)

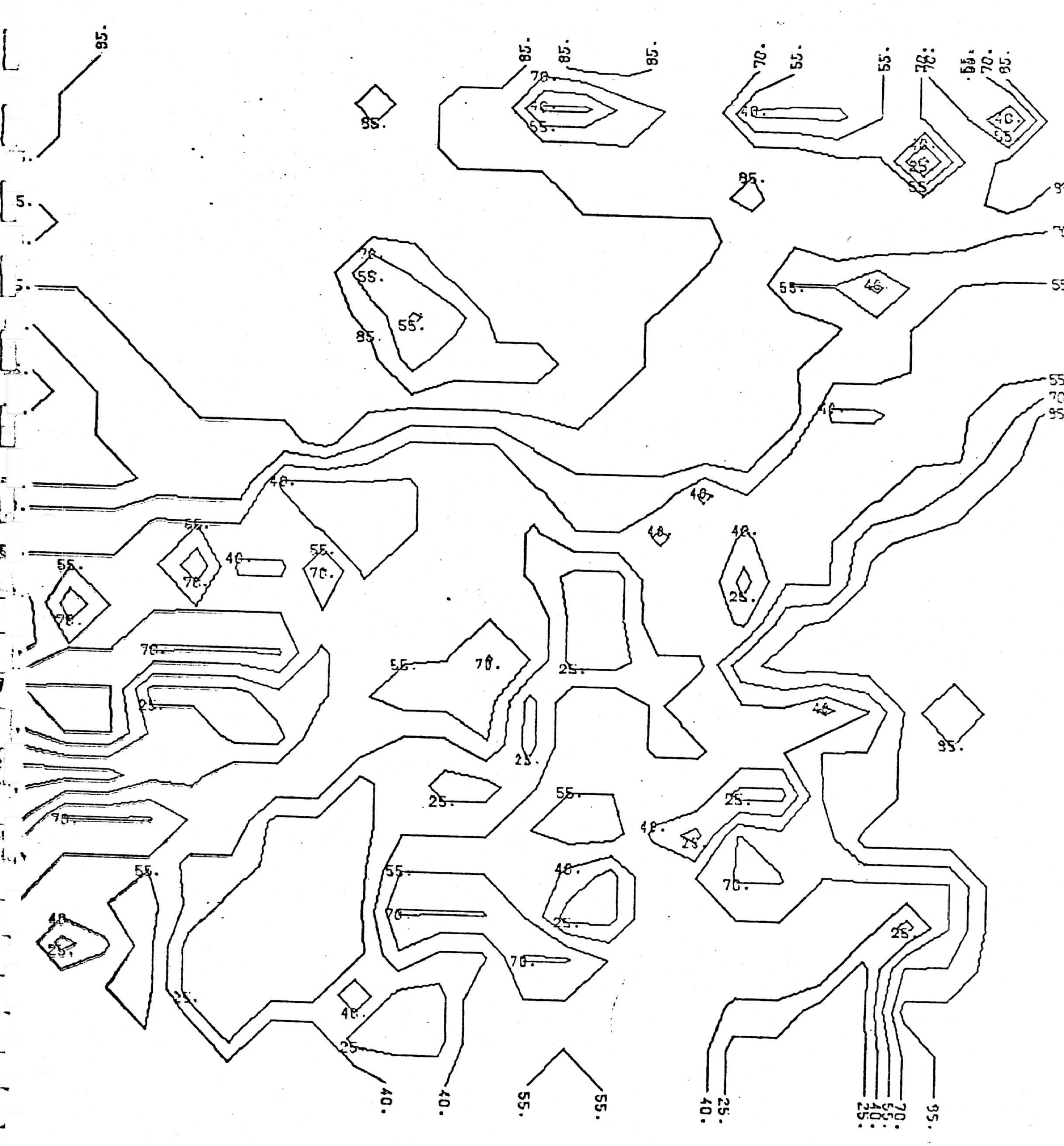

% of clear sounding samples is quite small except for subgrids 2 and 12. Also, most subgrids contain a significant amount of both cloud types.

2. <u>Use of an Internal Space View to Measure VAS Telescope Offset</u>

Using the notation described on page 7 in Monthly Progress Report No. 7 (March) and assuming that

$R_{d,1} = R_{d,2} = R_{d,3} = R_0 = R_f = 0$, the apparent radiance of an external blackboy at temperature T_E is given by

$$N_{eff} = B(T_E)R_1R_2R_3\tau_f(1 - K) + B(T_1)\varepsilon_1R_2R_3\tau_f(1 - K) + B(T_2)\varepsilon_2R_3\tau_f(1 - K) + B(T_3)\varepsilon_3\tau_f + B(T_0)R_3\tau_fK + B(\tau_f)\varepsilon_f \tag{2-1}$$

where $R_i = R_{s,i}$ has been used as in Report No. 7. If the external blackbody is empty space, then the expression becomes

$$N_{eff}^{(T=0)} = B(T_1)\varepsilon_1R_2R_3\tau_f(1 - K) + B(T_2)\varepsilon_2R_3\tau_f(1 - K) + B(T_3)\varepsilon_3\tau_f + B(T_0)R_3\tau_fK + B(T_f)\varepsilon_f \tag{2-2}$$

During calibration with shutter at temperature T_s the equivalent external blackbody is defined by the requirement

$$B(T_s) = B(T_E)R_1R_2R_3\tau_f(1 - K) + N_{eff}^{(T=0)} \tag{2-3}$$

which can also be expressed as

$$B(T_E) = \frac{B(T_s) - N_{eff}^{(T=0)}}{R_1R_2R_3\tau_f(1 - K)} \quad . \tag{2-4}$$

If a space viewing mirror could be inserted at point s, the $N_{eff}^{(T=0)}$ term could be almost directly measured without knowing the temperatures of the primary optical components. The radiance observed during the internal space view is given by

$$N_0 = (1 - R_4)B(T_4) \tag{2-5}$$

while the radiance observed at point s through the primary optics is just

$$N_{eff}^{(T=0)}$$

Thus the zero level and thus $N_{eff}^{(T=0)}$ can be established to within the accuracy of the determination of $(1 - R_4)B(T_4)$, i.e.

$$N_{eff}^{(T=0)} = X_0 + N_0 \qquad (2\text{-}6)$$

where X_0 is the measured response difference beteeen the two space looks and N_0 is the correction term. Under these conditions we have

$$B(T_E) = \frac{B(T_s) - X_0 - N_0}{R_1R_2R_3\tau_f(1 - K)}, \text{ or} \qquad (2\text{-}7)$$

$$B(T_E) = [B(T_s) - X_0 - (1 - R_4)B(T_4)]\cdot[R_1R_2R_3\tau_f(1 - K)]^{-1}. \qquad (2\text{-}8)$$

If we expand all Planck functions about T_s, then we obtain the relation

$$T_E = T_s + [\frac{\partial B(T_s)}{\partial T}]^{-1} B(T_s) \frac{R_4 - R_1R_2R_3\tau_f(1 - K) - X_0/B(T_s)}{R_1R_2R_3\tau_f(1 - K)}$$

$$- \frac{(1 - R_4)\cdot(T_4 - T_s)}{R_1R_2R_3\tau_f(1 - K)} . \qquad (2\text{-}9)$$

For T_s = 300°K selected Planck functions and derivatives are tabulated below

ν	$B_\nu(T_s)$ [mW/(m²-ster-cm⁻¹)]	$\frac{\partial B_\nu}{\partial T_s}$ [mW/(m²-ster-cm⁻¹-°K)]	$B_\nu/(\frac{\partial B_\nu}{\partial T})$ [°K]
2700 cm^{-1}	0.558	0.0241	23.17
1490 cm^{-1}	31.08	0.741	41.95
895 cm^{-1}	118.36	1.717	68.94
680 cm^{-1}	149.29	1.688	88.47

Obviously, the second term, involving the derivative function, is dominant; a 1% uncertainty in R_4 alone can result in an uncertainty of 0.88°K in T_E (ν = 680 cm^{-}). Including the uncertainties in R_1, R_2, R_3, τ_f, and (1 - K) appear to make this use of an internal space view impractical because of the large errors introduced, even when the measured value X_0 is error free.

In order to understand more clearly how this unexpected result comes about, it is useful to consider a simple case in which the VISSR is isothermal. If we further assume that all temperatures and R_4 are perfectly known and that X_0 is perfectly measured then the following conditions apply

$$B(T_E) = B(T_s) \tag{2-10}$$

$$X_0 + N_0 = (1 - \tau)B(T_s) \tag{2-11}$$

$$B(T_E) = \frac{1}{\tilde{\tau}}[B(T_s) - (X_0 + N_0)]$$

$$= \frac{\tau}{\tilde{\tau}} B(T_s) \tag{2-12}$$

where $\tau = R_1 R_2 R_3 \tau_f (1 - K)$ (2-13)

and where $\tilde{\tau}$ indicates a value of τ which contains errors. Equation (2-12) is the equation which makes use of the space look to obtain $\tilde{T}_E$ (which has the exact value T_E). Since the error containing parameter $\tilde{\tau}$ must be used in applying this equation, the result will be in error also. By expanding the Planck functions of equation (2-12) we obtain the condition

$$\tilde{T}_E - T_E = \left(\frac{\tau}{\tilde{\tau}} - 1\right) \frac{B(T_s)}{\left(\frac{\partial B(T_s)}{\partial T}\right)} \tag{2-14}$$

Thus a 1% error in $\tilde{\tau}$ yields up to 0.88°K error in $\tilde{T}_E$; and larger errors are more than possible since there are five factors in $\tilde{\tau}$ which must be estimated.

The calibration using measured temperatures and a model of the primary optics emission is generally more accurate than the calibration using an internal space view to measure primary optics emission because the former approach yields errors which cancel as the isothermal condition is approached. This is not true for the second method.

3. Use of an Internal Space View to Determine In Flight Values of VAS Optical Constants

There remains the possibility of using the internal space view to determine in-flight values of the optical constants used in the temperature dependent calibration model. This amounts to solving the linear system of equations

$$N_k(T=0) = \sum_{i=1}^{5} D_i B(T_{i,k}) \qquad (3\text{-}1)$$

where $N_k(T=0)$ is a measurement of $X_0 + N_0$ when the optical components (i=1,5) have temperatures $T_{i,k}$, i.e. k is an index of measurement sets. Both $N_k(T=0)$ and $B(T_{i,k})$ have implicit wavelength dependence. Consider a measurement set of k-1,K different temperature measurement sets and corresponding $N_k(T=0)$ measurements. Then equation (3-1) can be written in matrix form as

$$N = D \cdot B , \qquad (3\text{-}2)$$

where N and D are row vectors with components

$$(N)_k = N_k(T=0), \; k=1,K \qquad (3\text{-}3)$$

$$(D)_i = D_i \quad , \; i=1,5 \qquad (3\text{-}4)$$

and where B is a 5 x K matrix of radiances with components

$$(B)_{ik} = B(T_{i,k}) \; . \qquad (3\text{-}5)$$

The least squares solution for the vector of optical constants D is given by

$$D = NB^T(BB^T)^{-1} \qquad (3\text{-}6)$$

provided that the matrix BB^T has an increase. A minimum but not sufficient condition is that $K \geq 5$. The error in the D_i's will depend on the measurement errors in the $T_{i,k}$'s and the N_k's as well as the variability of the temperature gradients observed. The best solution will be obtained for widely varying temperature situations and for K >> 5. This will minimize the chance for obtaining a singular or near singular (very small eigenvalues) matrix BB^T. Further analysis is required to determine if the D vector of optical constants can be solved with sufficiently small error to yield an improvement relative to the original estimates.